



The New Wuqing 70m Radio Telescope and Measurements of Main Electronic Properties in the X-band

De-Qing Kong^{1,2}, Chun-Lai Li^{1,2,*}, Hong-Bo Zhang^{1,2}, Yan Su^{1,2}, Jian-Jun Liu^{1,2}, Xin-Ying Zhu^{1,2}, Jun-Duo Li¹,
Xi-Ping Xue¹, and Chen Li¹

¹ Key Laboratory of Lunar and Deep Space Exploration, National Astronomical Observatories, Chinese Academy of Sciences, Beijing 100101, China; licl@bao.ac.cn

² University of Chinese Academy of Sciences, Beijing 100049, China

Received 2021 November 5; revised 2021 December 9; accepted 2021 December 24; published 2022 February 18

Abstract

The new Wuqing 70 m radio telescope is first used for the downlink data reception in the first Mars exploration mission of China, and will be used for the other deep space communications and radio astronomical observations in the future. The main specifications and measurement results of some properties in the X-band are introduced in this paper, such as pointing calibration, gain and efficiency, system noise temperature, system equivalent flux density, and variations with elevation. The 23 parameters pointing calibration model considering the atmospheric refraction correction in real time is presented in the telescope, and the pointing accuracy reaches $5''.70$ in azimuth direction and $6''.07$ in elevation direction for different weather conditions. More than 62% efficiencies are achieved at full elevation range, and more than 70% in the mid-elevation. The system equivalent flux density of the X-band in the mid-elevation reaches 26 Jy.

Key words: telescopes – astronomical instrumentation, methods and techniques – atmospheric effects

1. Introduction

The Wuqing 70 m radio telescope (WRT70), 70 m in diameter, is located at the Wuqing Station of the National Astronomical Observatories, longitude 117.10 E, latitude 39.54 N, and elevation 8 m. The WRT70 is a turntable Cassegrain antenna with an Azimuth-Zenith mounting support-structure, and is currently the largest fully movable single dish antenna in Asia. The construction of the WRT70 started in 2018 October, started trial operation in 2020 October and was passed the final reception test in 2021 February.

The WRT70 is first used for the downlink data reception in the first Mars exploration mission of China, and will be used for other deep space communications and radio astronomical observations in the future. The frequency of the downlink signal is X-band in the first Mars exploration mission of China. In the subsequent missions, Ka-band will be used for the downloading of the scientific data. So in the design of the WRT70, the position of the Ka-band is reserved, and the accuracy of the mount and panel has been also considered. The WRT70 has three feeds working at S/X, X and Ku-bands now, and Ka and K or C-bands will be installed later. The feeds can be rotated quickly to the right position automatically to change the observing frequency. In the Mars and following deep space probes, the WRT70 is arrayed with the Miyun 50 m, Miyun 40 m and Kunming 40 m radio telescopes, which makes the equivalent aperture of the synthesized antenna reach 103 m.

It is necessary to test the main electronic properties for a new telescope, such as pointing calibration, gain and efficiency, system noise temperature, system equivalent flux density, and variations with elevation. For large telescopes, pointing calibration needs to be carried out first (Meeks et al. 1968; Yuan et al. 1986; Himwich 1993). The linear calibration model is applied in the pointing calibration of mostly large radio telescopes (Meeks et al. 1968; Yuan et al. 1986; Zhang et al. 2009). However, the linear model does not take the structure nonlinear errors into considerations. The pointing model based on Least-square support vector machines was presented in 2007 (Zhang et al. 2007), and the model based on generalized extended interpolation was presented and used in the Miyun 50 m radio telescope in 2008 (Kong et al. 2008), which can partially solve the nonlinear problem. The model considering the nonlinear error of azimuth-axis was presented and used in the Kunming 40 m radio telescope in 2014 (Kong et al. 2014). Due to the improvement of pointing accuracy of large antennas, higher requirements are put forward for the atmospheric refraction model.

Calibrations and measurements of the mainly properties of the WRT70 in the X-band were performed from 2020 November to 2021 January. In Section 2, the results show that the WRT70 fully meets the design specifications and has excellent performance compared with large-diameter antennas. The pointing calibration method and result will be introduced in Section 3. The antenna gain and efficiency are measured at full elevation by radio sources. The results of efficiency and gain will be introduced in Section 4. The results of system

* Corresponding author.

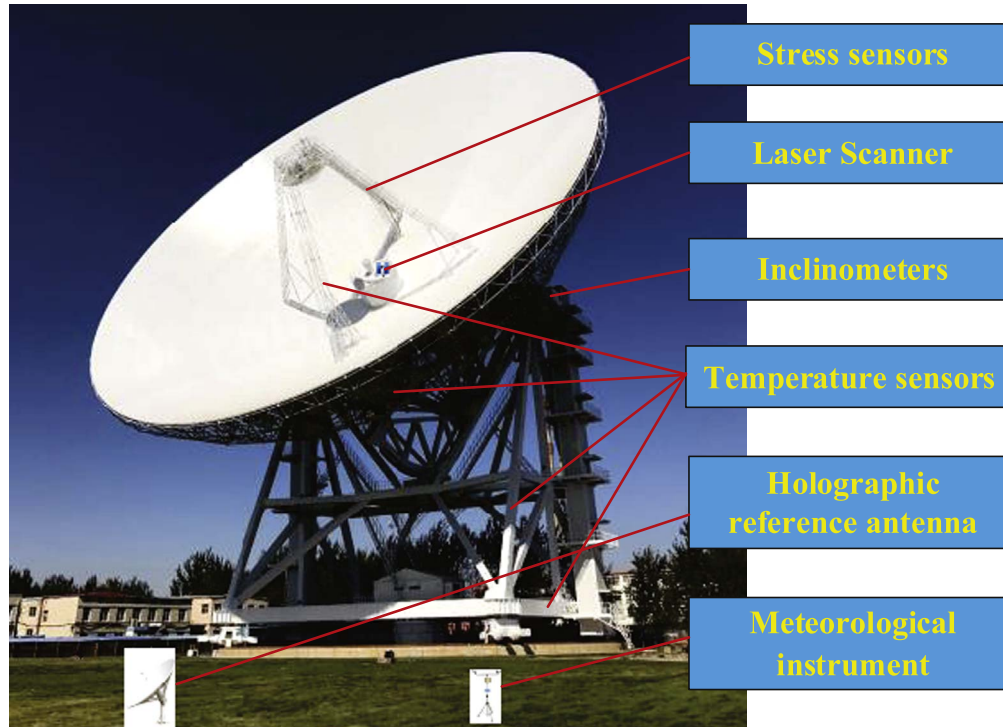


Figure 1. The WRT70 Radio Telescope.

temperature and its variations with elevation will be introduced in Section 5. The results of the system equivalent flux density and variations with elevation using the Y -factor method by radio source will be introduced in Section 6.

2. The Main Specifications of the WRT70

The parabolic reflector is made from solid plate in all the 70 m region. The accuracy of the main surface is 0.35 mm (elevation 48° , by actual measurement), and the accuracy of the secondary reflecting surface is 0.16 mm which is relatively easy to ensure. The main reflective surface dispersion support structure with umbrella-shaped reflector back frame is adopted. The influence of uniformity improves the accuracy of the reflection surface. In the accuracy measurement and adjustment of the main reflection surface, the innovative combination of photographic method and laser scanning method is used, which not only improves the accuracy and speed of surface measurement, but also makes it easy to achieve surface measurement at different elevation angles. The photogrammetry is used in the pre-adjustment of the antenna panel, which can only be carried out at night and takes a long time. The advantage of the laser scanner is that the measurement time is as short as a few minutes. The laser scanner is used to measure the main and sub-reflector surface deformation at different elevation angles, which is mainly used for the preliminary adjustment curves of the sub-surface and the research of the measurement of sunshine temperature surface deformation.

The main and sub-reflector surface shaped design technology is adopted, which is to optimize the antenna parameters, the radiation level at the edge of the sub-reflector surface, and the aperture field distribution function of the primary reflecting surface. The sub-reflector surface follow-up and the best anastomosis technologies are adopted in the WRT70 design, which ensuring the accuracy of the main reflector surface in the full elevation. The sub-reflector has three adjustment degrees of freedom which are Y and Z -axis translation, and rotation around X -axis. The repetitive positioning accuracy of Y , Z and X -axis is 0.08 mm, 0.08 mm and $5''$ respectively, then the pointing error caused by the sub-reflector repetitive accuracy is less than $0''9$. As a result, the calculated antenna efficiency of the X -band is greater than 70% near the panel adjusting positions, and more than 60% within the full elevation.

Because of the huge structure, the long control line and the very heavy wind load, the servo control equipment is susceptible to interference and the control accuracy is not easy to guarantee. The full digital control loop technology and multi-motor (azimuth eight motors, pitch four motors) electric anti-gap and the Linear Quadratic Gaussian anti-gust disturbance control technologies are adopted, and the high control accuracy of $3''$ both azimuth and elevation is achieved. Figure 1 shows the picture of the WRT70 radio telescope.

Because large antennas require high pointing accuracy and are easily affected by environmental factors, such as

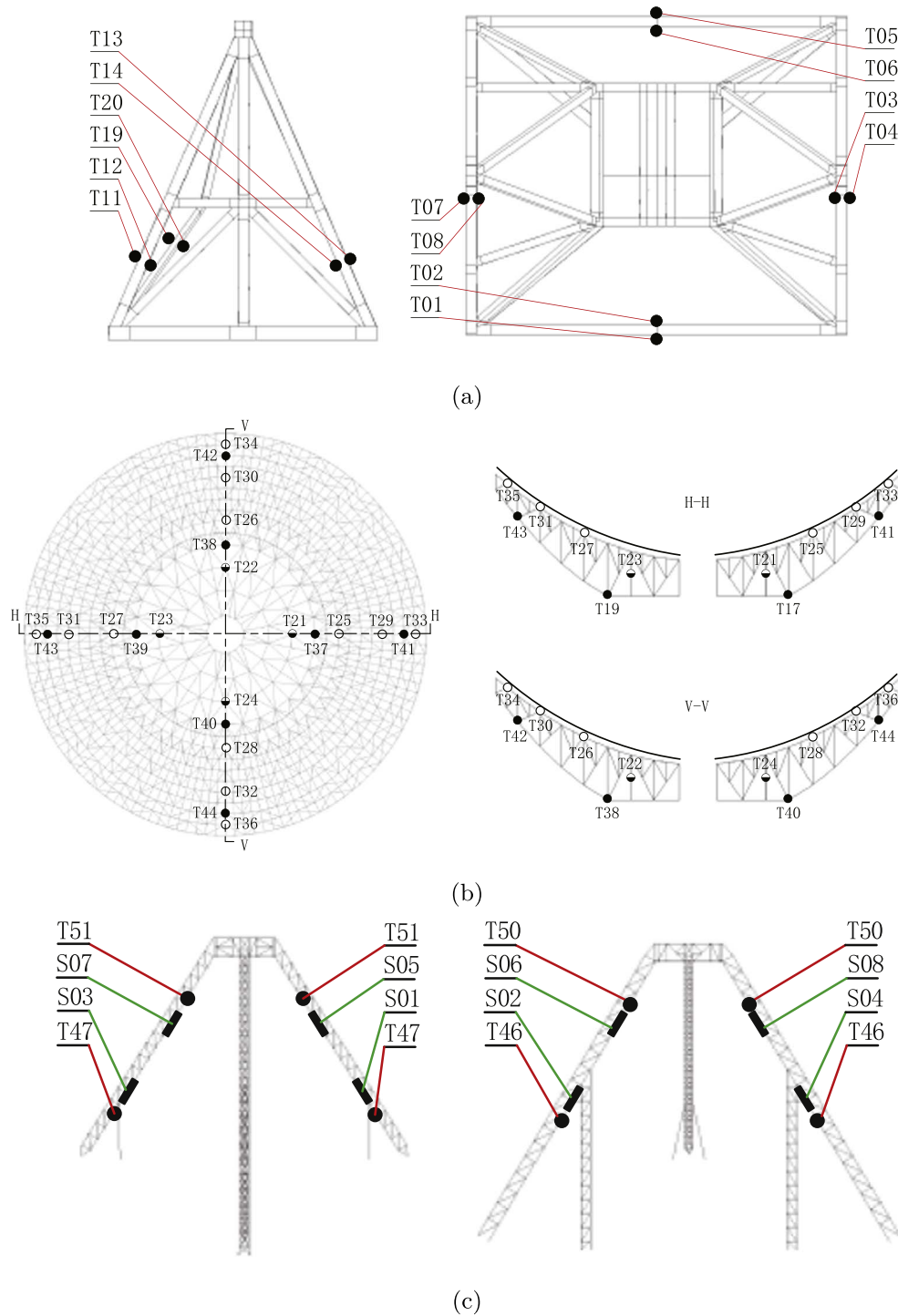


Figure 2. Partial temperature and stress sensors distribution. (a) Temperature sensors on the alidade, (b) temperature sensors on the main reflector, (c) temperature and stress sensors on the sub-reflector leg.

atmospheric refraction, wind and sunshine temperature, temperature sensors, inclinometers and weather meters are placed on key parts of the reflector and alidade. Two inclinometers are respectively installed near the elevation bearing of the alidade.

52 temperature sensors and eight stress sensors are placed on the telescope, which will be used for long-term monitoring and correction experiments on structural deformation. The stress sensors are used for the research on wind load and gravity

deformation, and the temperature sensors are used for the research on sunshine temperature deformation. Figure 2 shows the temperature and stress sensors distribution. A 23 parameters correction model considering nonlinearity and the atmospheric refraction correction in real time improves the pointing accuracy of the WRT70, which can be used in real scientific observation.

Table 1 gives the main specifications of the WRT70.

3. The Pointing Calibration

Pointing accuracy is one of the most important performance indicators in large radio telescopes. System pointing calibration is the first step for a new telescope. The widely used linear pointing calibration model is expressed as (Zhang et al. 2009)

$$\begin{cases} \delta A_1 = C_1 - C_3 \tan(E) \cos(A) \cos(C_4) - C_3 \tan(E) \sin(A) \sin(C_4) + C_5 \tan(E) \\ \quad - C_6 \sec(E) \\ \delta E_1 = C_2 + C_3 \sin(A) \cos(C_4) - C_3 \cos(A) \sin(C_4) + C_7 \cos(E) + C_8 / \tan(E). \end{cases} \quad (1)$$

Here, δA_1 and δE_1 are the azimuth and elevation calibration functions, the correction factor $C_1 \sim C_8$ can be identified by the least squares method.

For large radio telescopes, it is necessary to adopt a more complex correction model, because of the nonlinear errors produced by the antenna structure, the influence of sunshine and wind load. For the WRT70, based on the pointing model considering the nonlinear error of azimuth-axis of Kunming 40 m radio telescope (Kong et al. 2014), we add the azimuth and elevation encoder scale error terms to correct the errors due to coaxiality of encoder installation. The pointing calibration model we used is expressed as

$$\begin{cases} \delta A_n = a_1 - a_2 \tan(E) \cos(A) - a_3 \tan(E) \sin(A) + a_4 \tan(E) - a_5 \sec(E) \\ \quad + a_6 A + a_7 \tan(E) \cos(2A) + a_8 \tan(E) \sin(2A) + a_9 \tan(E) \cos(A) \cos(2A) \\ \quad + a_{10} \tan(E) \sin(A) \cos(2A) + a_{11} \cos(E) + a_{12} \sin(E) \\ \delta E_n = e_1 + e_2 \sin(A) - e_3 \cos(A) + e_4 \cos(E) + e_5 / \tan(E) + e_6 E - e_7 \sin(2A) \\ \quad + e_8 \cos(2A) - e_9 \sin(A) \cos(2A) + e_{10} \cos(A) \cos(2A) + e_{11} \sin(E). \end{cases} \quad (2)$$

The parameters $a_1 \sim a_{12}$ and $e_1 \sim e_{11}$ in Equation (2) are correction factors, and can be identified by the least squares method, and a_6 and e_6 are respectively the azimuth and elevation encoder scale differences. The traditional atmospheric refraction correction model is only for one atmospheric condition without considering the influence of real-time changing factors such as atmospheric temperature, atmospheric pressure, and relative humidity. The troposphere atmospheric refraction model in radio band given by Berman describes the

refraction angle at different elevation angles (Berman & Rockwell 1976). The atmospheric refraction angle of the entire troposphere to electromagnetic waves is calculated using the temperature, atmospheric pressure and relative humidity measured in real time on the ground. So the following elevation pointing calibration model considering the atmospheric refraction correction in real time is used in the WRT70

$$\begin{aligned} \delta E_z = & e_1 + e_2 \sin(A) - e_3 \cos(A) \\ & + e_4 \cos(E) + e_5 / \tan(E) \\ & + e_6 E - e_7 \sin(2A) \\ & + e_8 \cos(2A) - e_9 \sin(A) \cos(2A) \\ & + e_{10} \cos(A) \cos(2A) + e_{11} \sin(E) \\ & + R(T, P, RH, E). \end{aligned} \quad (3)$$

Here (Berman & Rockwell 1976)

$$\begin{aligned} R(T, P, RH, E) \\ = F_p F_t F_w \left(\exp \left\{ \frac{\sum_{j=0}^8 K_{j+3} [U(Z)]^j}{1 + \Delta_3(Z)} \right\} - K_{12} \right) \end{aligned} \quad (4)$$

and

$$\begin{aligned} F_p &= \left(\frac{P}{P_0} \left\{ 1 - \frac{\Delta_1(P, Z)}{1 + \Delta_3(Z)} \right\} \right), \\ F_t &= \left(\frac{T}{T_0} \left\{ 1 - \frac{\Delta_2(T, Z)}{1 + \Delta_3(Z)} \right\} \right), \end{aligned}$$

$$\begin{aligned} U(Z) &= \left\{ \frac{Z - K_1}{K_2} \right\}, \\ F_w &= \left(1 + \frac{W_0 RH}{TP} \left\{ \exp \left(\frac{W_1 T - W_2}{T - W_3} \right) \right\} \right), \end{aligned}$$

$$\Delta_1(P, Z) = (P - P_0) \{ \exp [A_1(Z - A_2)] \},$$

Table 1
The Main Design Specifications of the WRT70

Items	Indicators
Diameter	70 m
Feed form	Cassegrain type
Frequency/bandwidth	S: 2.15 ~ 2.31 GHz X: 7.6 ~ 9.2 GHz Ku: 10.95 ~ 12.75 GHz
Antenna efficiency (Elevation $\geq 10^\circ$)	S: $\geq 60\%$, X: $\geq 60\%$, Ku: $\geq 50\%$
Antenna temperature (at feed output point, and when polarizer at normal temperature)	S: ≤ 40 K, X: ≤ 35 K, Ku: ≤ 42 K @ elevation 30° ; S: ≤ 52 K, X: ≤ 45 K, Ku: ≤ 55 K @ elevation 10°
Point accuracy (r.m.s.)	Ku: $\leq 9''$ (wind ≤ 8 m s $^{-1}$, temperature change $\leq 2^\circ\text{C h}^{-1}$); X/S: $\leq 13''$ (wind ≤ 8 m s $^{-1}$, temperature change $\leq 5^\circ\text{C h}^{-1}$); Ku(reserved): $4''$
Movable range	Azimuth: $\pm 270^\circ$, Elevation: $+5^\circ \sim +90^\circ$
Maximum slewing speed	Azimuth: $0^\circ 5$ s $^{-1}$, Elevation: $0^\circ 3$ s $^{-1}$
Slewing speed under accuracy controlling	Azimuth: $0.003 \sim 0^\circ 3$ s $^{-1}$ Elevation: $0.0015 \sim 0^\circ 15$ s $^{-1}$
Maximum acceleration	Azimuth: $0^\circ 25$ s $^{-2}$, Elevation: $0^\circ 15$ s $^{-2}$
Acceleration under accuracy controlling	Azimuth: $0^\circ 002$ s $^{-2}$, Elevation: $0^\circ 002$ s $^{-2}$
Surface accuracy (r.m.s.)	0.60 mm
Optics	Prime focus, $F/D = 0.30$

$$\Delta_2(T, Z) = (T - T_0) \{ \exp [B_1(Z - B_2)] \},$$

$$\Delta_3(Z) = (Z - C_0) \{ \exp [C_1(Z - C_2)] \}.$$

Here R is the angle of refraction, Z is the actual zenith angle, E is the elevation angle, P is the local atmospheric pressure, T is the local temperature, RH is the relative humidity, and other parameters are constant terms.

The observation was taken in the X-band, since the Ku-band receiver is not installed at that time. Sources selected for calibration observation are strong intensity, small angular diameter, and uniform distribution in the sky. The selected radio sources are 3C 273B, 3C 286, 3C 380, 3C 279, 3C 380, 3C 345, DR21, 3C 84, etc.

The pointing errors in total 149 positions, were observed in 2021 November in the first round pointing correction. The pointing calibration results of the WRT70 are shown in Table 2, where e_1 is the residual pointing error after the calibration using the linear pointing calibration model (Equation (2)), and e_2 is the error using the calibration model (Equation (3)). It can be seen from Table 2 that e_2 is better than e_1 . Particularly, the elevation-axis pointing accuracy increases

Table 2
Comparison of the First Round Pointing Residuals (Rms) of the WRT70

	$e_1/('')$	$e_2/('')$
Azimuth	5.57	5.29
Elevation	5.63	4.93
Total	7.92	7.23

from $5''63$ to $4''93$ and improves by 12.4%. The overall pointing accuracy increases from $7''92$ to $7''23$ and improves by 8.7%. Figure 3 shows the sky coverage of the pointing calibration observations and the distribution of the pointing calibration residues of the first round pointing calibration.

In order to be suitable for different weather conditions, we carried out the second round of measurements considering the correction of atmospheric refraction. The pointing errors in total 199 positions were observed in 2021 January. In order to ensure the pointing correction has a wide range of adaptability, observation time covered different weather conditions such as sunny, cloudy, moderate rain and snow. The influenced by the uneven temperature in sunny daytime was not considered in pointing calibration. The pointing calibration results of the WRT70 is shown in Table 3, where e_1 is the residual pointing error after the calibration using the linear pointing calibration model (Equation (1)), e_2 is the error using the calibration model (Equation (2)), and e_3 is the error using the calibration model (Equation (3)) with the real-time atmospheric refraction model. Figure 4 shows the pointing sky coverage, the calibration residues, temperature, relative humidity and atmospheric pressure distributions of the second round calibration.

Table 4 shows the rms values of the two models (Equations (2) and (3)). The overall pointing accuracy increases from $6''73$ to $6''07$ and improves by 9.8% by using the real-time atmospheric refraction model. In particular, in the observation of low elevation angles below 20° , the pointing correction residual reduces by 19.3%, 23.1% lower than 15° , and 27.5% lower than 10° . The new model makes the elevation correction residuals at different elevation more at the same level, the low elevation angle pointing accuracy deterioration caused by atmospheric refraction is basically eliminated.

4. Gain and Gain Variation with Elevation

The gain curve with elevation was measured from 10° to 80° elevation of WRT70. In the measurement of the Miyun 50 m radio telescope, the radio source Cyg A was used as the measurement beacon, and the effect of Cyg A broadening was removed (Zhang et al. 2009). Because the beamwidth of WRT70 is only $130''$, it is not suitable for the measurement of the 70 m antenna. We selected 3C 84 as the beacon, since it is almost the strongest radio point source in X-band. The Y-factor of 3C 84 in the X band of WRT70 exceeds 3 dB, so higher gain measurement accuracy can be obtained.

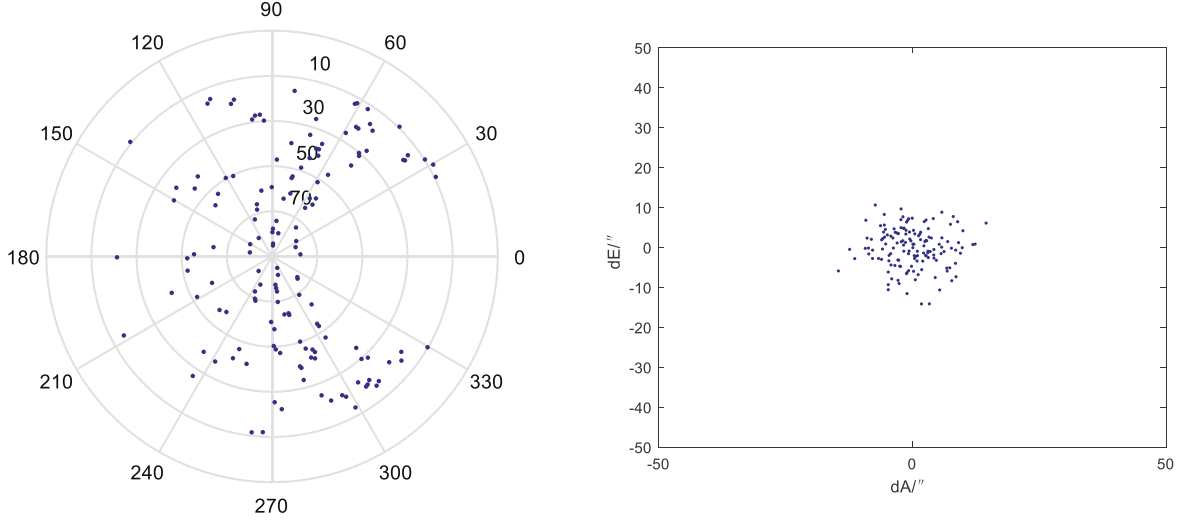


Figure 3. The sky coverage of the pointing calibration observations and the distribution of the pointing calibration residues of the first round pointing calibration.

Table 3

Comparison of the Second Round Pointing Residuals (Rms) of the WRT70

	$e_1/('')$	$e_2/('')$	$e_3/('')$
Azimuth	5.99	5.70	5.70
Elevation	6.99	6.73	6.07
Total	9.21	8.82	8.33

Azimuth and elevation planes are scanned respectively. Normally the beam shape of large antennas at the X band can be presented well by a Gaussian function. Considering the influence of bottom noise and the change of ground noise, the constant term and the primary term are added in the antenna pattern fitting. So the fitting equation was taken as

$$y = p_1 e^{-(x-p_2)^2/p_3^2} + p_4 + p_5 x. \quad (5)$$

Here x is the distance to the radio source center, p_1, p_2, \dots, p_5 is the fitting parameters. Then the half and one-tenth beamwidth in the two planes can be measured by

$$\begin{aligned} \theta_{3dB_{Az}} &= 2(\sqrt{\ln 2} p_3 + p_2), \\ \theta_{10dB_{Az}} &= 2(\sqrt{\ln 10} p_3 + p_2). \end{aligned}$$

Figure 5 shows an example of the antenna pattern fitting of the scan in elevation direction of 3C 84 in the X-band. Figure 5(a) shows the raw observed pattern and fitting curve. Figure 5(b) shows the normalized observed pattern, fitting curve, and the residue.

Table 4

Pointing Calibration Residuals Under Certain Elevations

Elevation ($^\circ$)	Traditional (Rms, $''$)	Real-time (Rms, $''$)	Improved by (%)
≤ 15	10.22	7.85	23.1
≤ 10	10.13	7.35	27.5
≤ 20	9.31	7.52	19.3
≤ 25	8.72	7.34	15.8
≤ 30	8.66	7.35	15.2
≤ 35	8.29	7.11	14.1
≤ 40	8.02	6.96	13.1
≤ 45	7.71	6.75	12.4
≤ 50	7.60	6.67	12.2
≤ 55	7.37	6.49	11.9
≤ 60	7.14	6.30	11.7
≤ 65	7.02	6.24	11.1
≤ 70	6.97	6.24	10.4
≤ 75	6.80	6.10	10.3
≤ 80	6.79	6.10	10.2
≤ 85	6.74	6.08	9.8
≤ 90	6.73	6.07	9.8

The antenna gain was then calculated by the following equation (Zhang et al. 2009)

$$\begin{aligned} G(\text{dB}) = 10 \lg & \left[\frac{1}{2} \left(\frac{31000}{\theta_{3dB_{Az}} \theta_{3dB_{El}}} \right. \right. \\ & \left. \left. + \frac{91000}{\theta_{10dB_{Az}} \theta_{10dB_{El}}} \right) \right] - \Delta G_F - \Delta G_\sigma. \quad (6) \end{aligned}$$

Here, $\theta_{3dB_{Az}}$ and $\theta_{3dB_{El}}$ are the azimuth and elevation half-power beamwidth, $\theta_{10dB_{Az}}$ and $\theta_{10dB_{El}}$ are the azimuth and elevation one-tenth power beamwidth, ΔG_F is the feed loss,

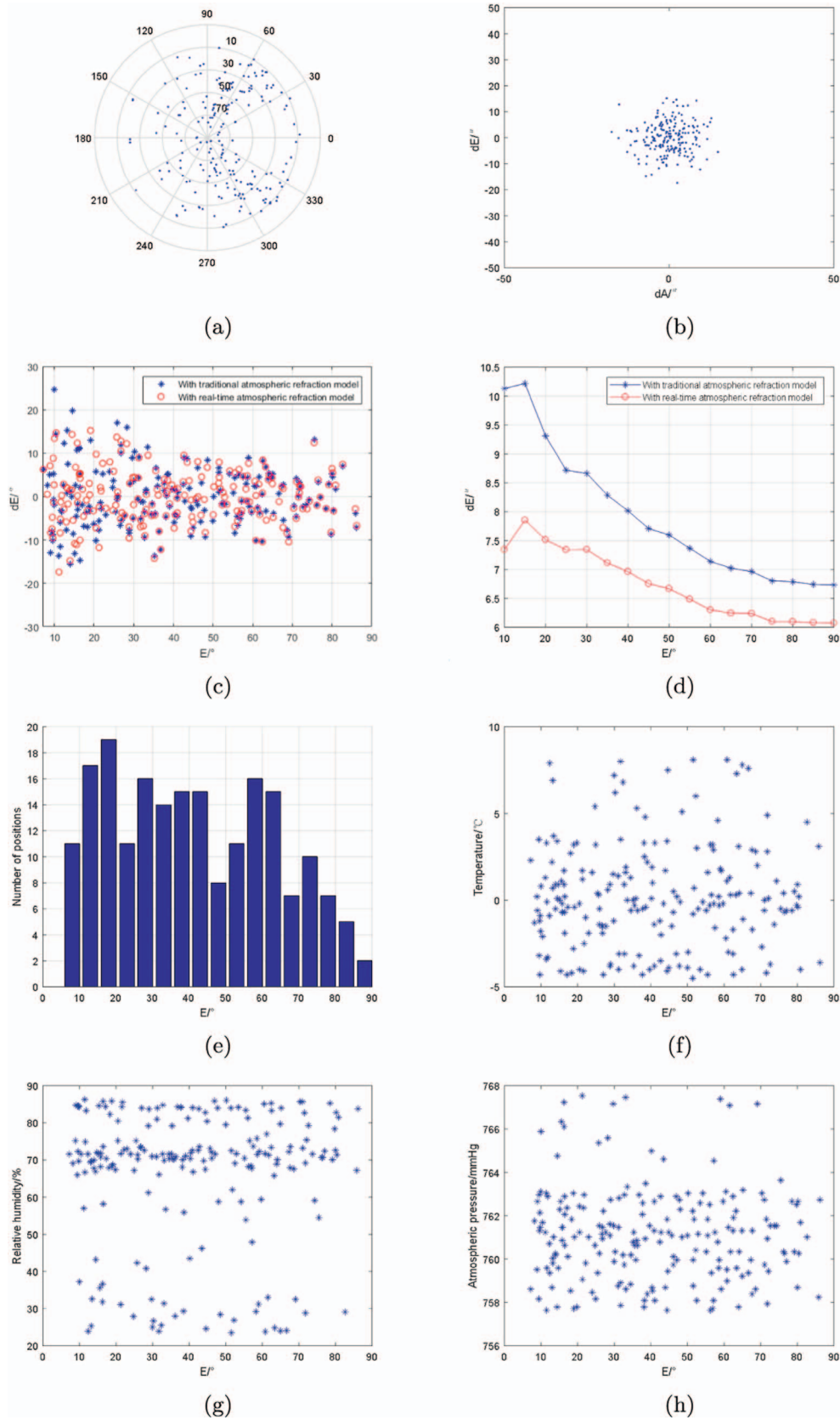


Figure 4. The second round pointing calibration with real-time atmospheric refraction. (a) The sky coverage of the pointing calibration observations, (b) the distribution of the pointing calibration residues, (c) pointing calibration residuals using or not using the real-time atmospheric refraction model, (d) residuals lower than certain elevation (rms), (e) number of positions in the 5° elevation range, (f) temperature distribution, (g) relative humidity distribution, (h) atmospheric pressure distribution.

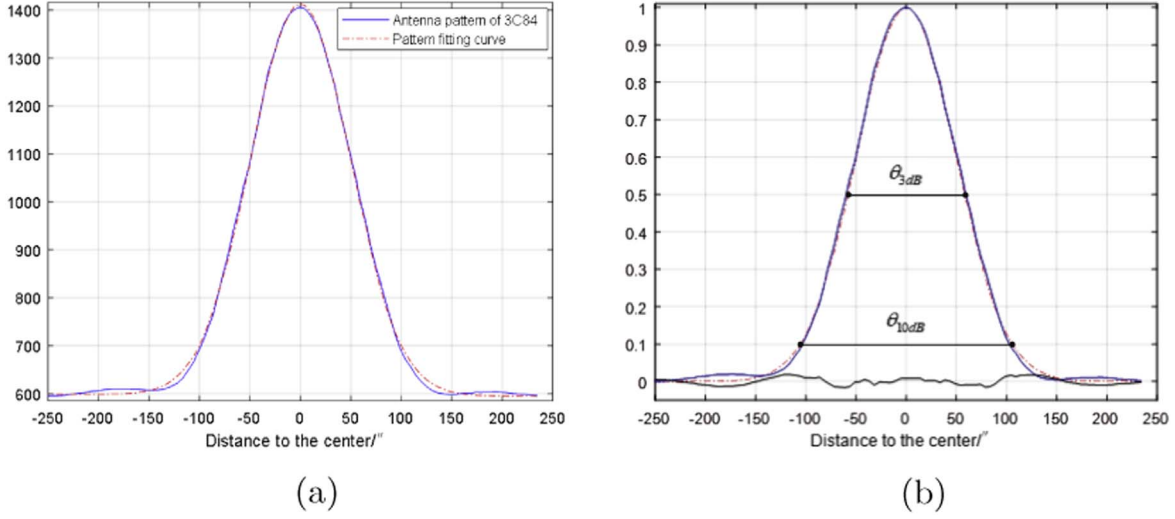


Figure 5. An example of the antenna pattern fitting of the scan in elevation direction of 3C 84 in the X-band, the continue line is the observed curve and the dashed line is the fitting curve. (a) The raw observed pattern and fitting curve, (b) normalized observed pattern and fitting curve, and the lower line is the residue.

$\Delta G_\sigma = 685.81 \left(\frac{\sigma}{\lambda}\right)^2$ is the surface accuracy loss, λ is the wavelength and σ is the antenna panel accuracy.

The method of the above gain variation measurement depends on the beams in the two perpendicular planes at different elevations. So the effect on gain measurements from atmosphere attenuation and system noise temperature error is very small. The observations were carried out in 2020 November, which were dry and clear days.

The efficiency and gain results are shown in Figure 6. The efficiency is from 62.4% to 74.0%, and correspondingly the gain is 73.7–74.5 dBi. The maximum efficiency and gain are at 46.9 elevation, which is close to the pre-adjusted position 48° elevation of the main surface.

5. The System Noise Temperature

The system temperature of a radio telescope comes from receiver noise, sky back-ground emission, ground emission, atmosphere emission, and antenna structure itself. For the case where both the polarizer and the field amplifier are cooled, system temperature can be expressed as the following equation

$$T_{\text{sys}} = T_r + \left(1 - \frac{1}{L_p}\right) T_D + \left(1 - \frac{1}{L_f}\right) \frac{T_0}{L_p} + \frac{T_{\text{sky}}}{L_p L_f}. \quad (7)$$

Here T_r is the equivalent temperature of the receiver at the LNA input port, T_D is the Dewar temperature, T_0 is the normal environment temperature, T_{sky} is the equivalent temperature contributed by the sky back-ground emission, ground emission, atmosphere emission, and antenna structure at the feed output,

L_p is the polarizer attenuation coefficient, and L_f is the feed attenuation coefficient without polarizer.

Because the polarizer is cooled, the waveguide port is not easy to disassemble. The Y-factor measurement method by covering the normal temperature load and pointing to the cold air at elevation 90° can obtain high accuracy (Wang et al. 2015). The measurement calculation equation is as follows

$$T_{\text{sys}} = \left[T_r + \left(1 - \frac{1}{L_p}\right) T_D + \frac{T_0}{L_p} \right] \cdot \frac{1}{Y}. \quad (8)$$

Here $T_r + \left(1 - \frac{1}{L_p}\right) T_D$ and L_p are measured together in the laboratory before the feed and receiver installation, Y is the Y-factor covering the load and pointing to the cold air.

We performed two sets of measurements. One set is a measure point at every 10° elevation intervals, and the other is a fast uniform rotation of the antenna from elevation 7° to 90°. The results are shown in Figure 7. The system temperature is from 48.8 to 25.8 K with the change of the elevation, and the two sets of measurements are basically the same.

6. System Equivalent Flux Density

System equivalent flux density (SEFD, J_y) is commonly used as the system sensitivity evaluation index in radio astronomy. The calculation formula can be expressed as (Wang et al. 2015)

$$\text{SEFD} = \frac{8kT_{\text{sys}}}{\eta\pi D^2 S_u}.$$

Here k is the Boltzmann constant, η is antenna efficiency, D is the antenna aperture and S_u is unit flow density (J_y). According

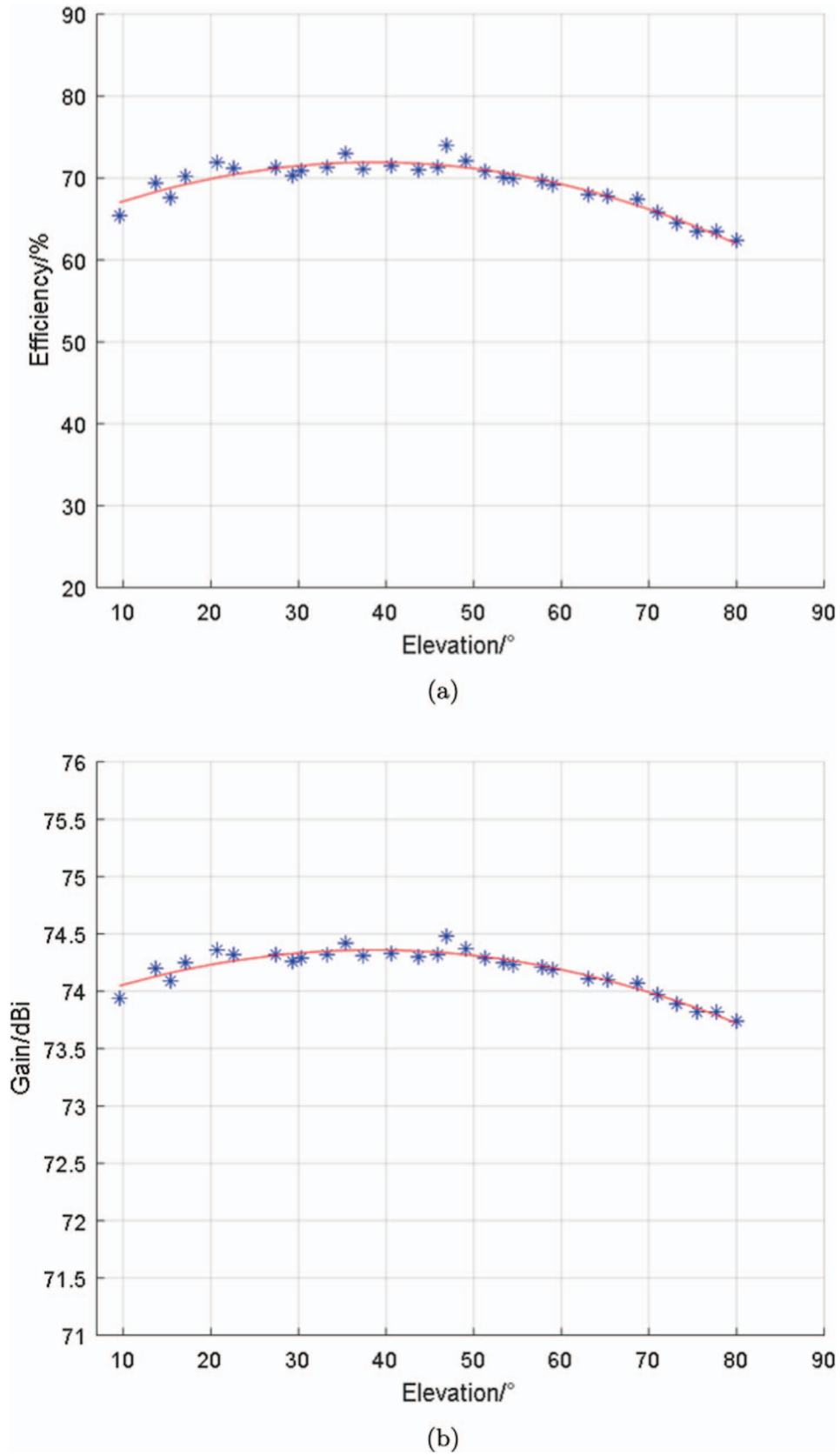


Figure 6. The X-band efficiency and gain of WRT70. (a) efficiency variation with elevation, (b) gain variation with elevation.

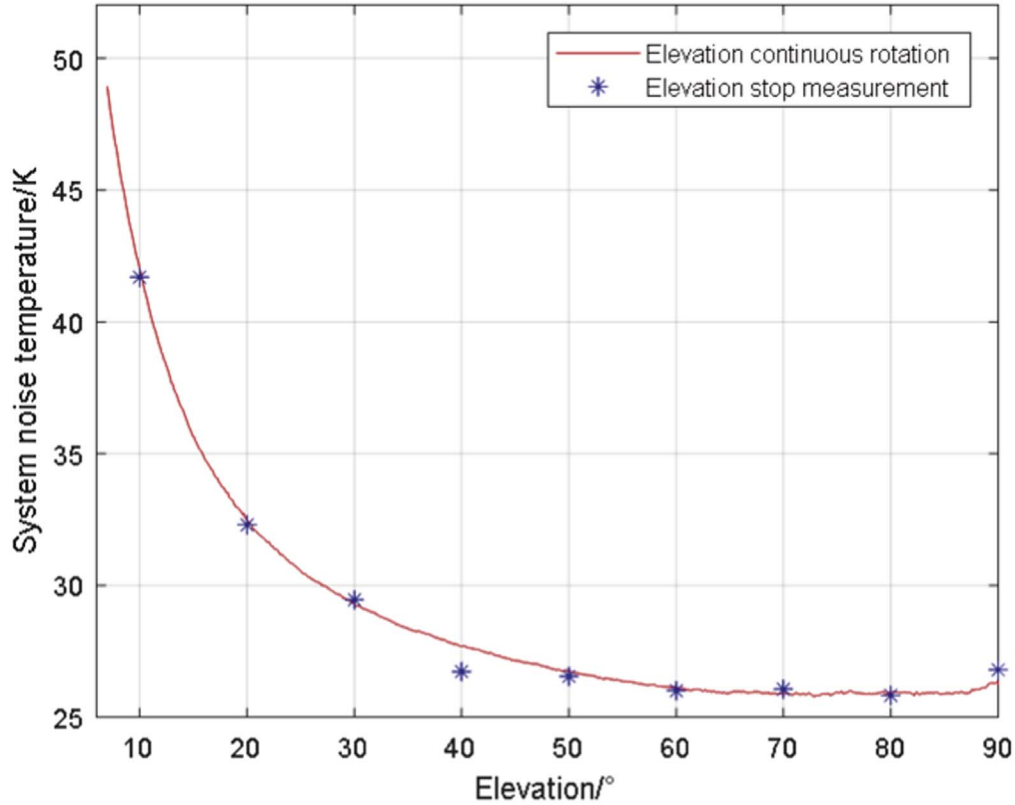


Figure 7. The X-band system temperatures of WRT70.

to the calculation formula of antenna gain, SEFD can be also expressed as the function of the quality factor G/T

$$\text{SEFD} = \frac{1}{G/T_{\text{sys}}} \cdot \frac{8\pi k}{\lambda^2 S_u}$$

Here λ is the wavelength. It can be seen that SEFD is determined if the antenna gain and system noise temperature are determined. By measuring the system noise temperature and antenna gain respectively, the measurement of SEFD can be realized. However, two measurements will increase error. So we used the on-off Y -factor method of radio source to measure SEFD directly. The major source of error in the measured SEFD is the uncertainty of the radio source flux density. The measured SEFD value can be expressed as

$$\text{SEFD} = \frac{S}{(Y-1)K_1K_2} \quad (9)$$

Here S is the flow of point radio source (Jy), Y is the on-off Y -factor, K_1 is the atmospheric attenuation correction factor and K_2 is the radio source expansion correction factor. We used the radio source DR21 as the beacon signal, which is almost the strongest point source of known accurate flux density. The flux

of DR21 in the X band has the form (Dent 1972)

$$S = 26.8 - 5.6 \lg \nu (\text{GHz}) \quad \text{for } \nu \geq 7 \text{ GHz.}$$

The measurement results of the X-band in right-hand-circular polarization are shown in Figure 8, which were measured on the evening of 2021 January, in dry and clear days. The minimum SEFD reached 25.8 Jy, less than 29.1 Jy above 30° elevations, and the maximum is 50.0 Jy at 7.3° elevation. It can be seen from Figures 7 and 8 that the change of SEFD with elevation is mainly affected by the system noise temperature.

7. Summary

The 23 parameters pointing calibration model considering the atmospheric refraction correction in real time is presented and used in the telescope, and the pointing accuracy reaches 5''.7 in azimuth direction and 6''.07 in elevation direction respectively for different weather conditions. The elevation overall pointing accuracy increases from 6''.70 to 6''.07 and improves by 9.8% by using the real-time atmospheric refraction model. In particular, in the observation of low elevation angles below 20°, the pointing correction residual reduced by 19.3%, 23.1% lower than 15°, and 27.5% lower than 10°.

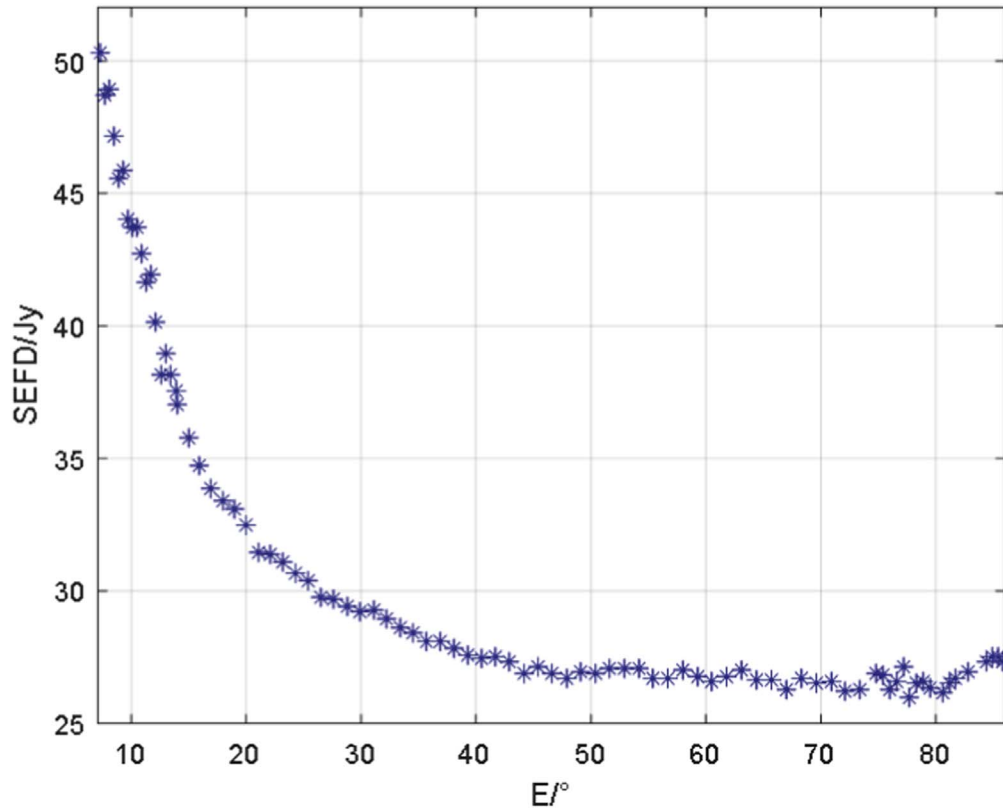


Figure 8. The X-band SEFD of WRT70.

The efficiency is from 62.4% to 74.0%, and correspondingly the gain is 73.7 to 74.5 dBi variations with elevation from 10° to 80° elevation. The system temperature is from 48.8 to 25.8 K variations with elevation from 7° to 90° elevation. The minimum SEFD reached 25.8 Jy, less than 29.1 Jy above 30° elevation, and maximum 50.0 Jy at 7.3° elevation. It can be seen that the WRT70 has high performance, and has been successfully applied in the first Mars exploration mission of China.

Acknowledgments

Authors thank Mr. Fan Wang and other operators for their assistance on the observations. This work was funded by the Astronomical Joint Fund of the National Natural Science Foundation of China and Chinese Academy of Sciences (U1831114).

References

- Berman, A. L., & Rockwell, S. T. 1976, New optical and radio frequency angular tropospheric refraction models for deep space applications, NASA STI/Recon Technical Report N, 1-31
- Dent, W. A. 1972, *ApJ*, **177**, 93
- Himwich, W. 1993, Operation Manual of VLBI Mark IV Field System Operation Manual of VLBI Mark IV Field System, NASA/Goddard Space Flight Center
- Kong, D. Q., Shi, H. L., Zhang, X. Z., & Zhang, H. B. 2008, *J. Xidian Univ.*, **35**, 157–61
- Kong, D.-Q., Wang, S.-G., Wang, J.-Q., Wang, M., & Zhang, H.-B. 2014, *RAA*, **14**, 733
- Meeks, M., Ball, J., & Hull, A. 1968, *ITAP*, **16**, 746
- Wang, J. Q., Zhao, R. B., Yu, L. F., et al. 2015, *AcASn*, **56**, 278
- Yuan, H. R., Peng, Y. L., & Xue, Y. Z. 1986, *Antenna Parameter Measurement Using Radio Astronomical Technique* (Beijing: Electronic Industry Press), 147
- Zhang, J. Y., Shi, H. L., Wang, W., et al. 2007, *Chinese J. Radio Sci.*, **22**, 804
- Zhang, X. Z., Zhu, X. Y., Kong, D. Q., et al. 2009, *RAA*, **9**, 367